THE JOURNAL OF PHYSICAL CHEMISTRY B

Article

pubs.acs.org/JPCB

Nanoscale Phase Analysis of Molecular Cooperativity and Thermal Transitions in Dendritic Nonlinear Optical Glasses

Daniel B. Knorr, Jr.,[†,‡] Stephanie J. Benight,[§] Brad Krajina,[†] Cheng Zhang,[∥] Larry R. Dalton,[§] and René M. Overney*,[†]

[†]Department of Chemical Engineering, University of Washington, Seattle, Washington 98195-1750, United States

[‡]Weapons and Materials Research Directorate, United States Army Research Laboratory, Aberdeen Proving Ground, Maryland 21009, United States

[§]Department of Chemistry, University of Washington, Seattle, Washington 98195-1700, United States

[∥]Department of Chemistry and Biochemistry, South Dakota State University, Brookings, South Dakota 57007-0896, United States

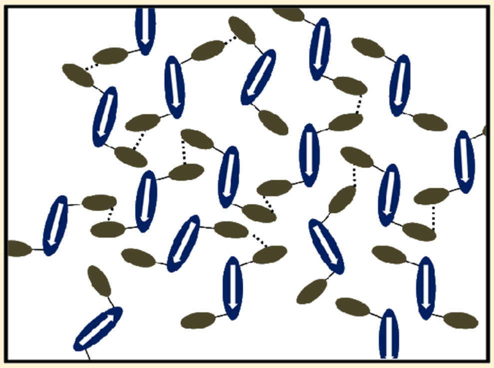

ABSTRACT: A broad nanoscopic study of a wide-range of dendritic organic nonlinear optical (NLO) self-assembly molecular glasses reveals an intermediate thermal phase regime responsible for both enhanced electric field poling properties and strong phase stabilization after poling. In this paper, the focus is on dendritic NLO molecular glasses involving quadrupolar, liquid crystal, and hydrogen bonding self-assembly mechanisms that, along with chromophore dipole−dipole interactions, dictate phase stability. Specifically, dendritic face-to-face interactions involving arene-perfluoroarene are contrasted to coumarin-containing liquid crystal mesogen and cinnamic ester hydrogen interactions. Both the strength of dendritic interactions and the impact of dipole fields on the relaxation behavior have been analyzed by nanoscale energetic probing and local thermal transition analysis. The presence of dendritic groups was found to fundamentally alter transition temperatures and the molecular relaxation behavior. Thermal transition analysis revealed that molecules with dendritic groups possess an incipient transition (T_1) preceding the glass transition temperature (T_2) that provides increased stability and a well-defined electric field poling regime ($T_1 < T < T_2$), in contrast to molecular groups lacking dendrons that exhibit only single transitions. On the basis of enthalpic and entropic energetic analyses, thermally active modes below T_1 were found to be intimately connected to the dendron structure. Their corresponding activation energies, which are related to thermal stability, increased moving from cinnamic ester groups to coumarin moieties to arene-perfluoroarene interacting groups. While dendritic NLO materials were found to possess only enthalpic stabilization energies at temperatures relevant for device operation ($T < T_1$), the apparent molecular binding energies above T_1 contain a substantial amount (up to ∼80%) of cooperative entropic energy. The multiple interactions (from dipole−dipole interactions to local noncovalent dendritic interactions) are discussed and summarized in a model that describes the thermal transitions and phases.

■ INTRODUCTION

Organic second-order nonlinear optical (NLO) materials are being actively pursued for applications in photonic devices such as high-speed electro-optic (EO) modulators, optical switches, and frequency converters.[1−5] For practical applications, NLO materials must have both high macroscopic EO activity, quantified by the r_{33} value, and thermal stability within the operating temperature range. High macroscopic EO activity can be achieved by acentrically ordering a system containing a high density of high-dipole chromophores via electric field poling at elevated temperatures.[1,6] In electric field poling, the initial state of the molecular system is isotropically ordered at random, and the system is heated, allowing for chromophore mobility. During heating, an electric field is applied, and the high-dipole chromophores align with respect to the electric field. Finally, the system is cooled in the presence of the electric field to obtain an acentrically ordered system. One challenge during the heating and poling process is to have sufficient spacing between the high-dipole chromophores to inhibit undesired spontaneous antiparallel pairing of the dipoles, which results in reduced EO activity.[7]

An apparent solution to reduce chromophore aggregation is to lower the loading density of the chromophores, which in turn, however, moderates the EO activity. A possible way to achieve a high loading density with minimal chromophore aggregation is the “site-isolation” approach,[6] where bulky constituents, e.g., dendrimers, are grafted to the chromophores. The dendrimers act as chromophore cages, thereby screening the electrostatic forces and shifting the overall shape of the chromophores from an anisotropic rod-like shape to a more

Received: July 25, 2012
Revised: October 15, 2012
Published: October 25, 2012

dx.doi.org/10.1021/jp307370y | J. Phys. Chem. B 2012, 116, 13793−13805

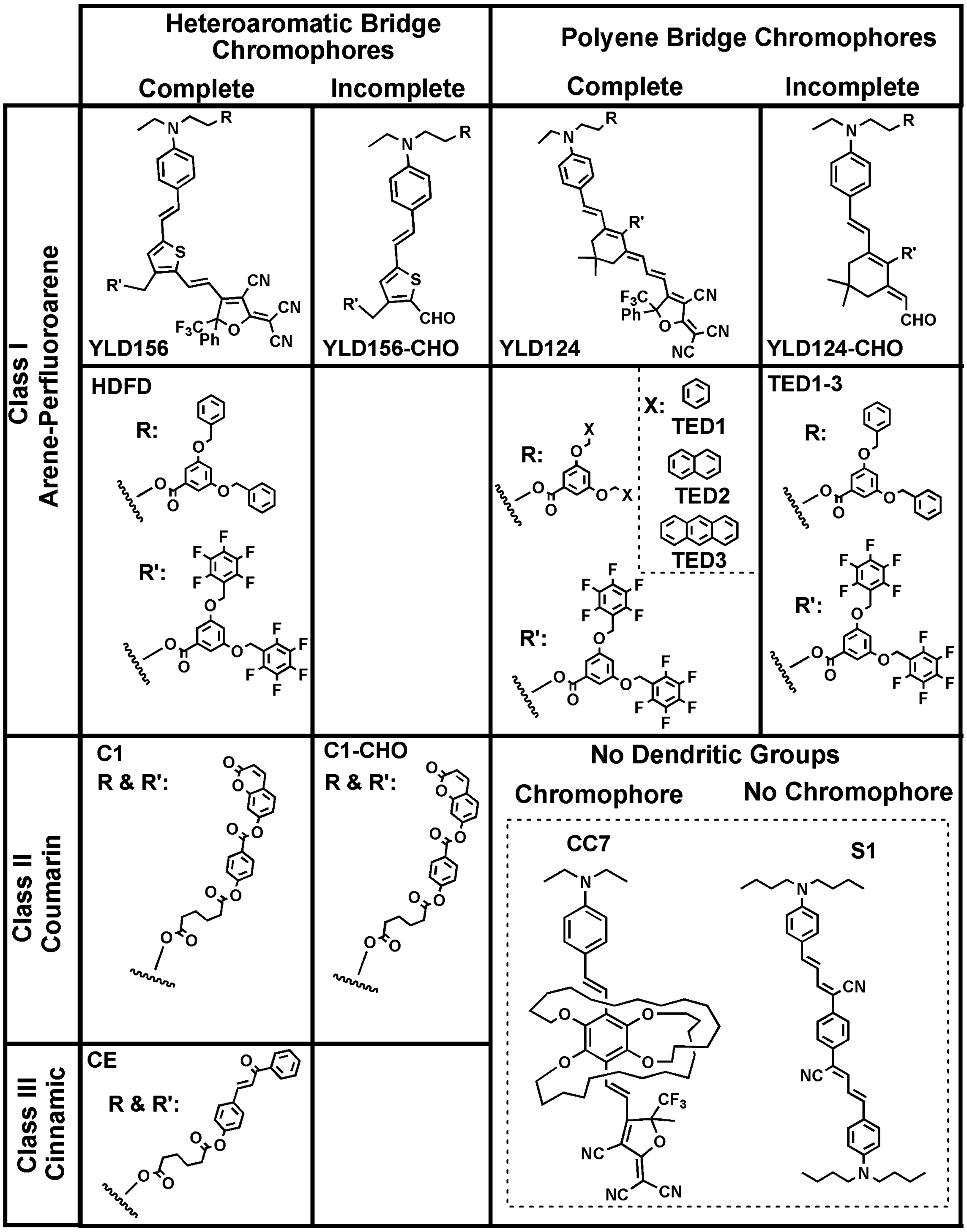

Figure 1. Molecules of interest for material Class I (**TED1**, **TED2**, **TED3**, **TED1A**, **TED1-CHO**, **HDFD**), Class II (**C1**, **C1-CHO**), and Class III (**CE**), as well as control molecules including a novel chromophore with a chain-containing bridge that has no dendritic groups (**CC7**) and a molecule that has no chromophore and no dendritic groups (**S1**) that is of similar size. Incomplete chromophores indicate materials without electron acceptor groups.

spherical one. This approach has been explored theoretically and experimentally and shows promising results.[2,6,8] Another approach to reduce dipole antiparallel pairing with high chromophore density involves self-assembled EO molecular glasses through strong arene-perfluoroarene ($Ar-Ar^F$) $\pi-\pi$ interactions to improve poling efficiency and chromophore alignment stability.[9−11] Materials of this nature resulted in EO coefficients exceeding those reported for NLO polymers.

For device operation, chromophore alignment imposed by electric field poling must be stable over long periods of time, i.e., alignment must exhibit thermal and temporal stability. As poled organic NLO materials are inherently nonequilibrium systems, the relaxation behavior and parameters that affect them, such as thermal transition temperatures, molecular energetics of thermally active modes, and molecular cooperative phenomena, have to be carefully analyzed.[10] Constraints must

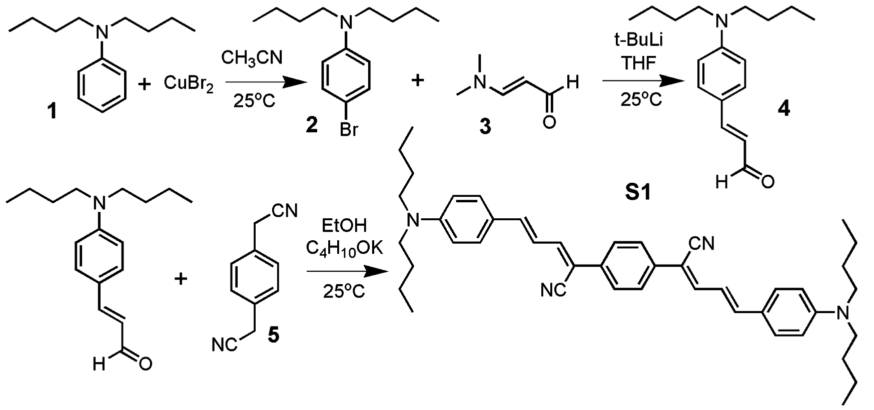

Figure 2. Synthesis of molecule **S1**.

be put in place on the molecular level to prolong the relaxation, i.e., delay the loss of chromophore acentric ordering for as long as possible.

Dendritic molecular glasses provide opportunities for nanoscale architectural control and molecular and supramolecular engineering to simultaneously improve macroscopic EO activity and thermal stability.[8,12,13] Recent efforts have focused on attached dendrons capable of self-assembly via internal constraints imposed via noncovalent interactions.[9,14] Along these lines, two separate material classes have been explored, (i) arene-perfluoroarene (Ar^{H}-Ar^{F}) interactions and (ii) liquid crystal (LC) forming moieties (e.g., coumarin mesogens). Both have shown great potential in improving the acentric order and therefore the macroscopic EO activity of naturally amorphous NLO systems.[9,15,16]

In the first material class, face-to-face interactions between perfluorinated and nonfluorinated aromatic rings are exploited to provide internal constraints. Along these lines, as shown in Figure 1, organic NLO molecular systems containing arene dendritic moieties (i.e., phenyl, naphthyl, or anthryl groups) and perfluoroarene (pentafluorophenyl groups) have shown excellent EO activity (>300 pm/V) and thermal stability.[14] This class of self-assembling amorphous NLO materials was found to exhibit very distinct temperature windows (bordered by thermal transitions) for optimum field poling.[9−11]

The second material system involves another strategy for providing temporal stability, wherein dendrons containing LC mesogens are used to enhance poling-induced order (Figure 1). In this strategy, specifically coumarin-based mesogens capable of reducing the dimensionality of the macroscopic chromophores system were employed.[15] Coumarin derivatives which form LC phases have been used extensively as alignment layers in LC displays[17] and in self-assembling monolayers.[18] These materials have the advantage that, apart from their ability to form LCs, they can also undergo photoinitiated cross-linking via the formation of cyclobutane dimers.[19−21] Coumarin-based mesogen systems generally form smectic *A* type LC phases in various polymers.[20,21] Along these lines, chromophores containing coumarin mesogens (C1) were synthesized.[22,23]

A third materials system is represented by the molecule CE, Figure 1, which, rather than the coumarin derivatives of C1, contains cinnamic ester derivatives that are traditionally used as photochromic dyes[24] and are not mesogenic.[25] Further, cinnamic acids and cinnamic acid ester derivatives have shown the tendency toward hydrogen bonding,[26,27] which provides the potential for self-assembly in this system.

In this study, correlations are established among the molecular mobility, critical transition temperatures, temporal (thermal) stability, and EO activity of electric field poled dendritic NLO glasses. It involves a comprehensive analysis of molecular systems considering an assortment of molecular system specific parameters, from the strength of the chromophore dipoles to a variety of dendritic interactions. The molecular mobility is addressed in terms of its energetic signature that possesses not only enthalpic activation barriers, but also, more notable in these glass-forming materials, a strong cooperative enthalpic signature. More specifically, arene-perfluoroarene dendritic systems and coumarin-based chromophore materials are discussed that both reveal three solid phases, separated by two distinct transitions.[10,11] It is the intermediate phase that strongly depends on the interactions involved, which provides the unique opportunity to engineer rationally, from the molecular scale up, organic solid NLO phases with distinct properties toward electric field poling. These two NLO systems are contrasted to less interacting NLO glasses, from systems with cinnamic dendritic groups, chromophore systems without dendritic groups, to a system that also lacks dipolar interactions. Beyond NLO materials, the concepts of physical interaction between small molecules that form amorphous glasses explored here is relevant for other material systems, for example, those used for three-dimensional lithography.[28]

EXPERIMENTAL SECTION

Materials and Synthesis. As pointed out, this study involves three classes of NLO chromophore materials that are distinguished by their dendritic groups. As illustrated in Figure 1, *Class 1* materials are composed of arene-perfluoroarene dendrons, with either heteroaromatic bridge chromophores, **YLD156**, or polyene bridge chromophores, **YLD124** or **YLD124-CHO**. The entire dendritic chromophore molecules are labeled in accordance with the literature,[9,10,14] as **HDFD**, **TED1**, **TED2**, **TED3**, or **TED1-CHO**. A selection of these NLO molecules are illustrated in Figure 1. *Class 2* materials entail coumarin dendrons, and either complete (**YLD 156**) or incomplete (**YLD 156-CHO**) heteroaromatic bridge chromophores. The molecules are correspondingly labeled **C1** and **C1-CHO**. *Class 3* materials contain cinnamic dendritic groups, and, as with **HDFD**, only complete heteroaromatic bridge chromophores (**YLD 156**). *Class 1−3* materials were synthesized according to the literature,[10,14,22,23,29] and are here contrasted with **CC7**, a NLO molecule that does not possess dendritic groups, and, **S1**, a nonpolar molecule that is deprived of not only a dipole moment, but also dendritic groups. The synthesis of **CC7**, introduced previously,[22] will be described in a future publication. Details about the synthesis of **S1** are provided below.

Thin films were produced by dissolving the sample materials in suitable solvents (trichloroethane, dichloromethane, chloroform, or toluene) at a concentration of about 10 wt %, filtering through a 0.2 μm PTFE-syringe filter, and then spin-coating onto indium tin oxide (ITO) glass or silicon substrates. The films with thicknesses of 0.5−1.0 μm were annealed overnight in vacuum at 25−70 °C, depending on the boiling point of the solvent and material glass transition temperature, to ensure the removal of any residual solvent.

For the synthesis of **S1** *N*,*N*-dibutyl aniline (97%, Aldrich), **1**, acetonitrile (HPLC grade, EMD), copper(II) bromide (99%, Aldrich), 3-dimethylaminoacrolein (90%, Aldrich), *tert*-butyl lithium (1.6 M in pentane, Acros Organics), tetrahydrofuran (EMD), 1,4-phenylenediacetonitrile (99%, Aldrich), and potassium *tert*-butoxide (1.0 M in THF, Aldrich) were used as received. Absolute ethanol (Deacon Laboratories) was stored with molecular sieve to ensure dryness. The reaction scheme is provided in Figure 2. 4-Bromo-*N*,*N*-dibutylaniline (**2**) was synthesized according to the literature.[30] Synthesis steps of the component (**4**) and (**S1**) are as follows.

*3-[4-(Dibutylamino)phenyl]-2-propenal (**4**).* The procedure used to synthesize **4** is quite similar to that described in the literature for an identical reaction wherein the only difference is the functionality of the tertiary amine.[31] In a flame-dried flask, under argon, 4-bromo-*N*,*N*-dibutylaniline (**2**) (10.72 g, 37.7 mmol) was dissolved in THF (290 mL) and was cooled to −78 °C. *tert*-Butyl lithium (75.4 mmol, 47 mL) was added, and the mixture was stirred for 5 min. 3-Dimethylaminoacrolein (189 mmol, 18.84 mL) was added and the mixture was stirred overnight until room temperature was reached. Saturated NH_4Cl was added to the reaction mixture, followed by extraction with ethyl acetate. Solvent was evaporated in vacuo and the product was purified by silica column chromatography using an ethyl acetate/hexanes (1:9) solvent affording 5.19 g product (53% yield).

*4-[1-Cyano-4-[4-(dibutylamino)phenyl]-1,3-butadien-1-yl]-a-[3-[4-(dibutylamino) phenyl]-2-propen-1-ylidene]-benzeneacetonitrile (**S1**).* The synthesis for this molecule (**S1**) is very similar to that described in the literature.[32] In a flame-dried flask, under argon, 1,4-phenylenediacetonitrile (**5**) (61 mg, 0.39 mmol) was dissolved in ethanol (25 mL) via stirring. Then, potassium *tert*-butoxide (3.12 mmol, 3.1 mL of 1 M solution in THF) was added. The system was allowed to stir for several minutes until the reaction mixture had a slightly bluish tint. 3-[4-(Dibutylamino)phenyl]-2-propenal (**4**) (0.202 g, 0.78 mmol) dissolved in ethanol (5 mL) was added, and the mixture was allowed to stir overnight at room temperature. Solvent was evaporated in vacuo and the product was purified by running silica column chromatography using an ethyl acetate/hexanes (1:9) solvent affording 59 mg of a black solid product (24% yield). ^{1}H NMR (300 MHz, $CDCl_3$) δ 7.52 (m, 4H), 7.40 (m, 4H), 7.25 (m, 4H), 6.98 (m, 2H), 6.64 (m, 4H), 3.32 (t, J = 6.0 Hz, 8H), 1.56 (m, 8H), 1.36 (m, 8H), 0.97 (t, J = 6.0 Hz, 12H). ^{13}C NMR ($CDCl_3$) δ 149.6, 143.3, 143.1, 134.0, 129.9, 125.8, 123.0, 120.3, 118.0, 111.8, 108.0, 51.1, 29.7, 20.6, 14.3. LRMS (ESI) (M^+, $C_{44}H_{54}N_4$): calc'd, 638.4; observed, 638.6 [M+Na].

Instrumental and Analysis. Thermal transition and relaxation temperatures were deduced from scanning-modulation force microscopy (SM-FM) plots[12,33,34] (Figure 3) involving a standalone scanning force microscope (SFM) (Explorer, Veeco, CA). Contact-mode silicon bar-shaped levers (PPP-CONT, Nanosensors, normal and lateral spring constants of ∼0.2 N/m and ∼80 N/m,[35,36] respectively) and a custom automated sample heating setup were used with a heating rate of 1 °C/min between steady-state recordings of thermomechanical sample responses. All SM-FM measurements were performed on spun-cast films at ambient pressure under a dry nitrogen atmosphere with relative humidities below 10% and a sinusoidal lateral force modulation frequency of ∼1 kHz. The cantilevers were geometrically preconditioned to reveal smooth, close to spherically shaped geometries.[10]

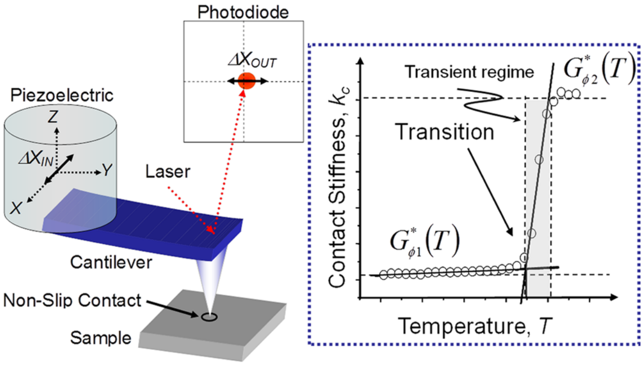

Figure 3. SM-FM setup and illustration of a typical SM-FM glass transition signature. Temperature transition values are obtained from "kinks" in contact stiffness versus temperature plots. The transient regime that identifies the heterogeneity of structural phases is bordered by the glass and rubber melt phase regimes, $\phi 1$ and $\phi 2$. $G^*(T)$ represents the dynamic complex modulus of the material.

SM-FM is a nonscanning SFM method, with which variations in the thermomechanical properties of materials are recorded as a function of the temperature. The experimental physical observable is the contact stiffness that includes the thermomechanical properties of the sample, i.e., the temperature dependent complex shear modulus $G^*(T)$, and the contact geometry.[34] The thermal gradient of the phase response, dG^*/dT, is geometry and rate dependent. Thermally activated transitions are determined from abrupt changes ("kinks") in the shear mechanical response curve, as illustrated in Figure 3 for a glass transition, which is one of several relaxation processes that can be recorded through SM-FM.

Glass transitions are well-known to cause a significant drop in the material's compressibility. This abrupt change causes the spherical SFM tip that is held at constant load to compress the material further, and thus, through contact area augmentation, results in a significant increase in the observed dynamic contact stiffness, k_c. In Figure 3, the regime identified as "transient regime" between the two phases, ϕk with k = 1,2, reflects to part the heterogeneity of two structural phases and the pressure nonequilibrium resulting from the time-steps in SM-FM experiments that are too short for the sluggish relaxation behavior in the heterogeneous regime of glass formers. In the case of polymers, the phase heterogeneity reflects a spatial distribution of independent backbone and side-chain relaxations. It is important to note that a material relaxation other than a glass or melting transition[37] can exist without noticeable transient regime, as we will discuss below. Differential scanning calorimetry (DSC) measurements were performed on a TA Q20 DSC at a heating rate of 10 °C/min.

Table 1. SM-FM Transitions in Dendritic NLO Materials Sorted by Increasing T_2

material	T_1 (°C)	T_2 (°C)	$T_2 - T_1$ (°C)	type of dendritic interaction
TED1-CHO[9,10]	41 ± 2	46 ± 2	5	Arene-perfluoroarene
C1-CHO[23]	42 ± 2	47 ± 2	5	Coumarin-coumarin (mesogenic)
CE	50 ± 3	59 ± 2	9	Hydrogen bonding
HDFD[11,14]	59 ± 2	70 ± 2	10	Arene-perfluoroarene
TED1[9,10]	59 ± 2	74 ± 2	15	Arene-perfluoroarene
C1[23]	61 ± 2	76 ± 2	15	Coumarin-coumarin
TED2[9,10]	75 ± 2	86 ± 2	11	Arene-perfluoroarene
TED3[9,10]	118 ± 2	126 ± 2	8	Arene-perfluoroarene

Table 2. SM-FM Transitions of Non-Dendritic Materials

material	T_2 (°C)	dendritic interactions	chromophores
CC7	60 ± 2	no	yes
S1	36 ± 1	no	no

The energetics of thermal active modes (e.g., side-chain rotations, molecular translations, or bonding/debonding events) were determined by intrinsic friction analysis (IFA),[38] involving the SFM (Explorer, Veeco Inc.) system described above, and operated under identical environmental conditions. SM-FM data provided the temperature phase regimes within which IFA was applied.

IFA is a spectroscopic rate method analogous to other techniques that probe molecular relaxations, such as dielectric spectroscopy, with the difference being that the velocity instead of the frequency is swept at constant temperature. The method has been applied successfully to polymers of wide complexity and thin films down to organic monolayers.[10,38−40] The observable in IFA is the friction force that entails the coupling phenomena between the one-dimensional sliding motion of the SFM probe and the thermally active modes within the material. If spectrally analyzed through IFA, the friction signal contains the enthalpic and entropic energies of the thermal modes, as discussed in detail elsewhere.[38] Briefly, the friction force is determined from the hysteresis in the torsional SFM deflection signal between forward and reverse scans as a function of the scan velocity at constant temperatures. These isothermal friction-rate curves are superimposed to an arbitrary reference isotherm by shifting them accordingly. From these shifts, the energetic information can be deduced based on the time−temperature superposition principle.[41−43]

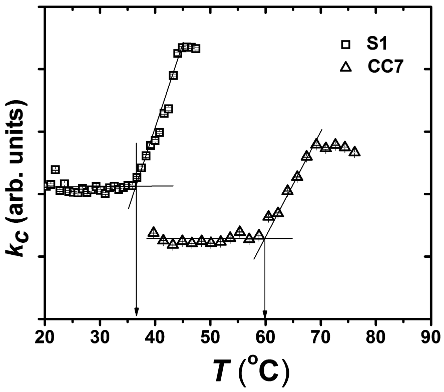

Figure 5. SM-FM results for **S1** and **CC7** revealing only single transitions for molecular glasses lacking dendritic interacting groups.

All dipole moment calculations were conducted using semiempirical VAMP geometry optimizations in Materials Studio as described previously.[10] Settings used were an NDDO Hamiltonian[44] with AM1* parameters,[45−47] a restricted Hartree−Fock formalism, a maximum step size of 1.0 Å, automatic multiplicity, and medium convergence tolerance.

■ RESULTS AND DISCUSSION

Transition Temperature Measurements. The thermal transition results of the SM-FM analyses for the dendritic NLO materials, as introduced in Figure 1, are provided in Table 1. Table 2 provides the transitions found for the nondendritic materials in this study for comparison. All dendritic systems possess two transitions, a finding that is in contrast to the nondendritic materials that possess only one transition. A SM-FM plot is provided for **CE** that is representative of all dendritic NLO materials in this study, Figure 4a. Figure 4b provides a contrasting sketch to Figure 3b. The second transitions at temperatures T_2 correspond to the transition temperatures determined by DSC, as shown in the inset of Figure 4a, and both DSC and SM-FM identify T_2 as a glass-like transition. Contrary to SM-FM glass transitions, the lower temperature

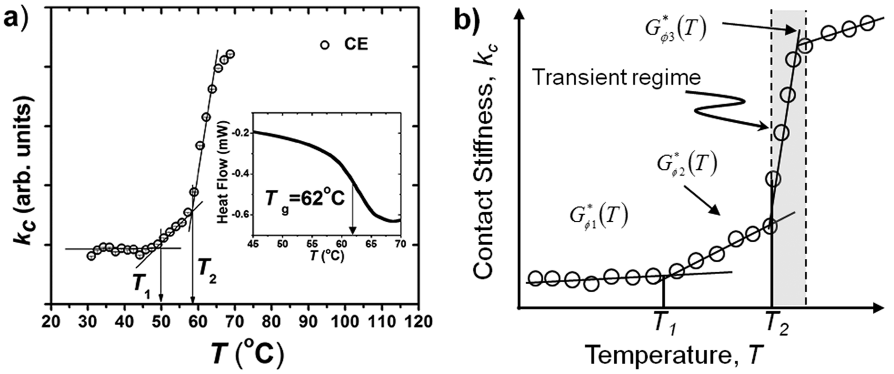

Figure 4. (a) Representative SM-FM plot of **CE** for dendritic NLO systems revealing two thermal relaxations in the dynamic contact stiffness (k_c) at $T_1 = 50 \pm 3$ °C and $T_2 = 59 \pm 2$ °C. Inset: DSC result for **CE**, with a transition at T_g of 62 °C, in good agreement with T_2. (b) Illustration of SM-FM plots for dendritic pendant group NLO systems highlighting the qualitative differences of the two transitions, and the three phase regimes.

Table 3. IFA Results and Calculated Dipole Moments of Dendritic NLO Materials Sorted by Increasing $E_{a,1}$[a]

material	$E_{a,1}$	$E_{a,2}$ (kcal/mol)	$E_{a,3}$	MW (g/mol)	ln ν_p @ T_{ref}	D_{calc} (D)
C1-CHO[23]	4 ± 3	26 ± 4	51 ± 4	1102.1	3.5	6.8 ± 2.5
CE	11 ± 2	33 ± 4	67 ± 4	1283.4	−0.1	11.0 ± 2.5
TED1-CHO[9,10]	13 ± 2	31 ± 4	55 ± 5	1212.1	2.1	9.7
C1[23]	16 ± 2	43 ± 4	72 ± 4	1399.4	−4.5	11.1 ± 2.7
HDFD[11,14]	23 ± 2	44 ± 3	71 ± 4	1427.2	−1.8	--
TED1[9,10]	25 ± 2	41 ± 2	69 ± 4	1509.4	−2.8	15.2
TED2[9,10]	29 ± 2	49 ± 3	82 ± 4	1609.5	−8.1	15.3
TED3[9,10]	35 ± 2	57 ± 5	98 ± 2	1709.6	−9.5	15.7

[a] T_{ref} = 49.5 °C; D = Debye.

Table 4. IFA Results of Non-Dendritic Materials, and Compilation of Chromophore Dipole Moments[a]

material	$E_{a,1}$ (kcal/mol)	$E_{a,3}$	MW (g/mol)	ln ν_p @ T_{ref}	D_{calc} (D)
S1	2 ± 1	45 ± 3	638.9	N/A	--
CC7	10 ± 2	66 ± 5	967.3	0.3	9.6 ± 0.3
YLD124 Chromophore[9,10]	--	--	--	--	12.7
YLD156 Chromophore	--	--	--	--	11.6
YLD124-CHO[9,10]	--	--	--	--	6.0
YLD156-CHO					5.4

[a] T_{ref} = 49.5 °C; D = Debye.

transitions, T_1, of dendritic materials do not show a transient regime, identifying the transition as a local phenomenon, such as an isolated side-chain rotation. The two transition temperatures T_1 and T_2 thereby reveal three thermal phase regimes, $G_{\phi\kappa}{}^*(T)$ with k = 1, 2, and 3.

The pendant group interactions responsible for causing a low temperature transition, and thus phase $\phi 2$, are, as per Tables 1 and 2, perfluoroarene (Ar^H-Ar^F) interactions for **HDFD** and the **TED** series,[10,11,14] coumarin LC interactions for **C1** and **C1-CHO**,[8] and hydrogen bonding, as found in this study for **CE** (Figure 4a). Hydrogen bonding for the pendant groups in **CE** is in accordance with studies involving cinnamic acids and cinnamic acid ester derivatives.[26,27] Specifically, hydrogen bonding can occur between C−H(aromatic)···O or C−H(olefinic)···O.[27,48] The two molecular systems lacking dendritic groups, i.e., **S1** and **CC7**, exhibit only single transitions (Figure 5). Thus, the second transition in NLO dendritic systems can be attributed to the interacting pendant groups of the NLO dendritic systems.

Energetic Relaxation Activation Analysis. A local energetic analysis via IFA was conducted to elucidate the three phases observed in dendritic NLO molecular systems, and to assess the impact of intermolecular constraints originating from dipole moments and pendant group interactions. The IFA results of the three classes of NLO materials from Figure 1 are compiled in Table 3. It provides phase specific energy values $E_{a,k}$ (k = 1, 2, 3) that correspond to the temperature regimes. The energetic information of the two nondendritic materials is listed separately in Table 4. In addition, both tables contain the calculated dipole moments of the entire molecules and of the chromophores alone.

With **CE**, an IFA data set representative of all dendritic NLO materials is provided and discussed. Figure 6a shows the friction−velocity isotherms of **CE** below T_1 = 50 ± 3 °C (c.f. Figure 4). A similar set of friction data exists between T_1 and T_2, and above T_2. Each set of friction isotherms was shifted horizontally (and vertically if necessary) to an arbitrarily chosen reference temperature, to produce a single overlapping master curve, as illustrated for **CE** in Figure 6b. The velocity spectroscopy master curve of the friction values reveals a relaxation peak at $\nu_p \approx 1$ nm/s for **CE** at a reference temperature of 49.5 °C, Figure 6b. It has to be noted that the reference temperature chosen here is below T_1 for **CE**, where the material is in its glassy state. This is in agreement with the other dendritic NLO systems with T_1 values above 49.5 °C, as verifiable by cross referencing Table 1 with Table 3. Dendritic systems with T_1 and even T_2 transition values below the reference temperature of 49.5 °C, such as **C1-CHO** and **TED-CHO** (Table 1), reveal higher relaxation velocities than found for glass phases, **CE**, **HDFD**, and **TED1−3** (Table 3).

Returning to Figure 6b, the horizontal shifts, known as shift factors ln a_T, were plotted versus the reciprocal temperature, in an Arrhenius-like fashion (inset of Figure 6b). The Arrhenius plot provides the energetic values $E_{a,k}$ (k = 1, 2, and 3) in accordance with

$$E_a = -R\left[\frac{\partial \ln(a_T)}{\partial(1/T)}\right]_p \qquad (1)$$

For instance, an energy value of $E_{a,1}$ of 11 ± 2 kcal/mol is deduced for **CE** below T_1, which can be attributed to the hydrogen bonding−debonding interaction between the cinnamic ester pendant groups,[26,27] distorted by the static dipolar interacting field, emanating from the strong chromophore dipoles, and the van der Waals (VdW) interactions of the network. Energy values for the higher temperature phases of **CE** or for other dendritic systems of this study are found in Table 3. It is important to note that the energy values can either be truly enthalpic or also possess a cooperative entropic component that is introducing a length scale over which the relaxation occurs, likely to exceed by orders of magnitude the molecular length scale.[40,49] As such, the energy E_a can be either an enthalpic activation energy or an apparent energy containing entropic and enthalpic components.

In relaxation processes, cooperative phenomena can manifest themselves in concerted molecular motions that involve entropic energies that originate from configurational adjustments. In polymers or strongly interacting molecular systems,

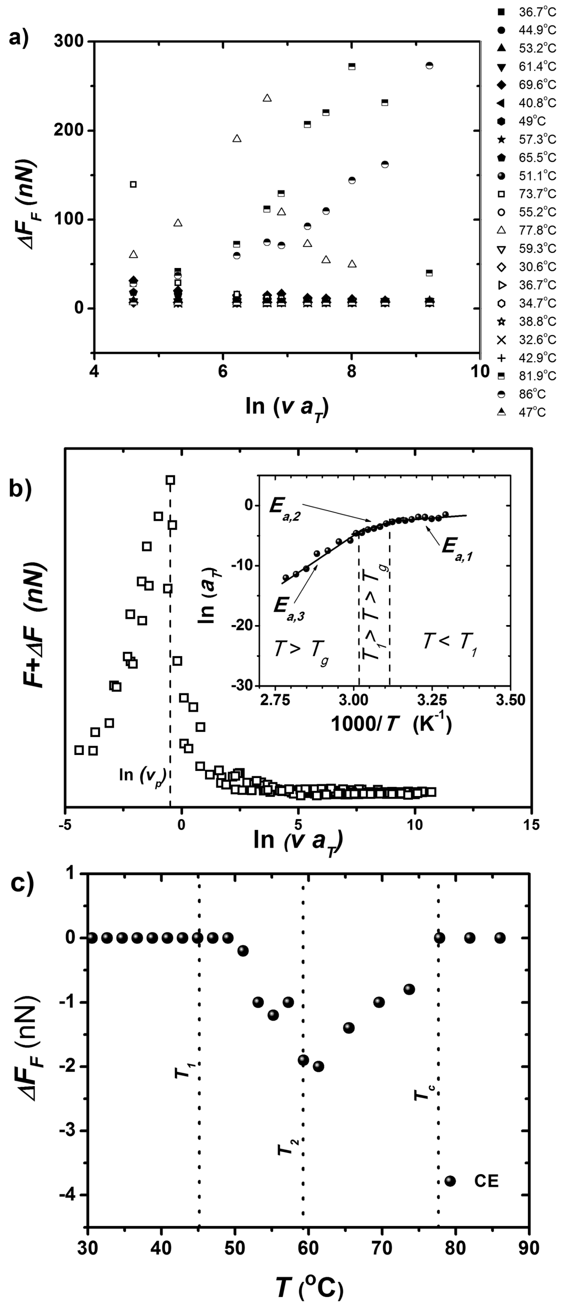

Figure 6. IFA results for **CE**: (a) Friction−velocity isotherms at indicated temperatures. (b) Shifted isotherms forming a master friction relaxation curve revealing the relaxation peak ln $\nu_p = -0.1$ at a reference temperature of 49.5 °C. (Inset) Arrhenius plots disclose the apparent activation energies $E_{a,1} = 11 \pm 2$ kcal/mol ($T < T_1$), $E_{a.2} = 33 \pm 4$ kcal/mol ($T_1 < T < T_2$), and $E_{a.3} = 67 \pm 4$ kcal/mol ($T_2 < T$). (c) Vertical force shift ΔF_F to collapse the isotherms on the master curve. T_1, T_2, and T_c represent the two transitions 1 and 2, and the temperature at which ΔF_F vanishes above T_2, respectively.

cooperative phenomena are observable during molecular aligning processes, such as shear flow or electric field poling. So, the energy E_a can be either an enthalpic energy or an apparent energy containing entropic and enthalpic components. It is the degree of vertical shifting (see Figure 6c) necessary to generate the master curve that determines the degree of cooperativity.[40,49]

From Figure 6c, with friction shift values close to zero below T_1, it can be inferred that for **CE** the hydrogen bonding−debonding reaction is solely enthalpic. This applies also to the two other classes of materials below T_1. For Class 1 (**HDFD** and **TEDs**) and Class 2 (**C1** and **C1-CHO**) materials, the interaction energies $E_{a,1}$ could be attributed to bonding−debonding interactions between the arene-pentafluorophenyl dendritic moieties and the coumarin pendant groups, respectively.[17,18,50−55]

As can be seen from Tables 3 and 4, the energy values $E_{a,k}$ increase for subsequent temperature regimes (i.e., for $k = 1$ to 3). The increase can be attributed to entropic cooperative energy contributions. As pointed out, the degree of cooperativity is also attainable by IFA.[49,40] Vertical force shifting ΔF_F in IFA is indicative of cooperativity in the system, i.e.,[49]

$$\Delta F_F \approx -\frac{T\Delta S^*}{\phi'} \tag{2}$$

where ϕ' is the contact area normalized stress activation volume.[49] On the basis of the nonzero shift values above T_1 of Figure 6c, which is representative of all dendritic materials listed in Figure 1, energies above T_1 carry both enthalpic and entropic contributions. The origin for enthalpic interactions is temperature invariant, so the difference between the phase energies can be solely attributed to changes in the entropic cooperativity. In the case of **CE** with $E_{a,2}$ and $E_{a,3}$ values of 33 ± 4 and 67 ± 4 kcal/mol, respectively, $T\Delta S^*$ can be determined to be 22 ± 4 and 56 ± 4 kcal/mol for the two thermal phases above T_1 and T_2, by deducting the enthalpic energy value of 11 ± 2 kcal/mol from the two apparent energies. Similarly high entropic contributions can be found for the other dendritic systems. At temperatures far above T_2 (i.e., at $T_c \approx T_2 + 20$ °C), the energies return to be purely enthalpic as they are below T_1 (Figure 6c), i.e., they have zero ΔF_F shift values.

The energies of primary significance for NLO applications are $E_{a,1}$ ($T < T_1$) and $E_{a,2}$ ($T_1 < T < T_2$), as they reflect the temporal stability under NLO operating conditions and the activation energy relevant for the poling process, respectively. The energy values $E_{a,3}$ provide information about the range of interactions in NLO networks. These three energy values are determined by the strength of the molecular dipole moments and the interaction strength between the pendant groups.

Figure 7 reveals the impact of the dipole moment on E_a values within the three thermal regimes. **C1-CHO** and **TED1-CHO**, which possess incomplete chromophores with significantly reduced dipole moments compared to their counterparts **C1** and **TED1**, reveal relatively low energies $E_{a,k}$ ($k = 1, 2, 3$). Thus, molecular NLO systems of chromophores with increased dipole moments can be expected to possess improved temporal stability, but are more difficult to pole. Also captured in Figure 7 is the impact of the dendritic interaction on the energetics. Within the TED series, the activation energies increase with increasing arene size, and more so for $E_{a,2}$ and $E_{a,3}$ than expected from the enthalpic interaction captured by $E_{a,1}$, and the slight increase in the dipole moment with larger pendant groups. Thus, while there is an increase in enthalpic interaction strength, given by $E_{a,1}$, increases due to entropic cooperative effects in $E_{a,2}$ and $E_{a,3}$ have to be considered. On the basis of the TED series, it can be concluded that the pendant-side group interactions not only alter the enthalpic energy, but also impact the molecular cooperativity within material phases to an even higher degree. The stark change in the dependence of the energetics on the dipole moments for the TED series illustrates

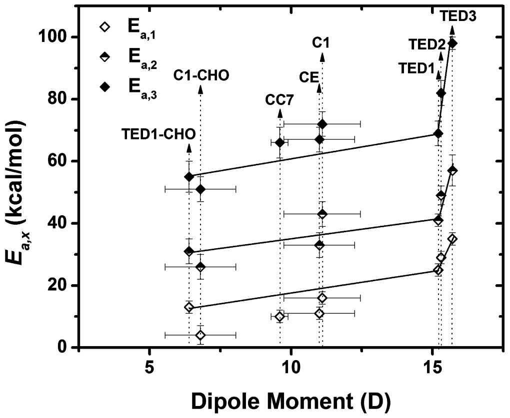

Figure 7. Dipole moment effect on the apparent activation energy for arene-pentafluorophenyl (**TED1**, **TED2**, **TED3**, **TED1-CHO**), LC (**C1** and **C1-CHO**), and hydrogen bonding interacting pendant groups (**CE**).

that changes in dendritic interactions are much more significant than changes in dipole moment.

Figure 8 shows that, besides the dipole moments and pendant group interactions, the molecular weight (MW) is also of importance in the energetics in NLO dendritic systems. Within the MW range studied, approximate linear relationships for $E_{a,k}$(MW) (k = 1, 2, 3) were found for all dendritic NLO systems introduced in Figure 1. To elucidate this initially unexpected behavior, we discuss the energy−molecular weight relationship in terms of a simplified structural grid model, as depicted in Figure 9.

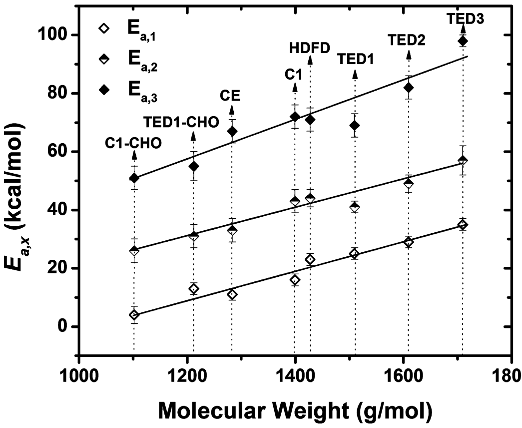

Figure 8. Energy−molecular weight relationship below T_1 and above T_2, i.e., $E_{a,1}$(MW), $E_{a,2}$(MW), $E_{a,3}$(MW), respectively. Linear fits reveal the following fit parameters: $E_{a,1}$(MW) = 0.049MW − 50, $E_{a,2}$(MW) = 0.049MW − 28, $E_{a,3}$(MW) = 0.069MW − 26.

In Figure 9a,b, we consider time snapshots of two dendritic NLO molecular systems of maximum packing densities, and identical system volume and temperature. The difference between Figure 9a and b is found in the molecular weight, or more specifically, the molecular number density, with low and high MW in Figure 9a and b, respectively. While the illustrations on the left in Figure 9a,b depict arbitrarily chosen arrangements of close-packed dendritic NLO molecules, the sketches on the right highlight the location of molecules (gray filled squares), (ii) the location of molecular bonds formed between pendant groups (filled dark circles), and (iii) molecules that lack any pendant group interaction (squares with diagonal lines) and are free to rotate or translate within the system. These two examples are representative of expressing the likelihood of finding mobile molecules, which increases with higher lower-molecular-weight molecules. From this model, it can be statistically expected that more "free" (unbound) molecules will be found in dendritic systems of lower MW than higher MW.

If we consider the bonds to be capable of bonding and debonding, we anticipate an increase in open bonds with increasing temperature. Consequently, a temperature can be reached at which the less dense molecular structure (Figure 9b) also exhibits mobile molecules. Considering that the transition temperatures T_1 and T_2 are distinct manifestations of the effect of the molecular mobility, we can expect low-molecular-weight NLO material to reveal lower transition temperatures than higher-molecular-weight materials. This is confirmed with the transition data in Table 1, if cross-referenced with the molecular weight information provided in Table 1. As the transition temperatures are intimately connected to activation energies, the presented simple model is in accordance with the finding presented in Figure 8 that yields an increase in the activation energy with increasing molecular size.

The heuristic model (Figure 9) finds further experimental support if we plot the logarithm of the molecular relaxation velocity, v_p, versus the corresponding activation energy $E_{a,3}$ at equivalent reference temperatures for the molecules of Classes 1 to 3. The plot displays a linear relationship, $E_{a,3}$ (ln v_p), for the molecules with interacting dendritic groups, which translates into a linear relationship of ln v_p with the molecular weight (Figure 10b). In contrast with the dendritic molecules are **CC7** and **S1**, i.e., molecules with missing pendant groups (Figure 10b), which show fundamentally different behaviors.

Apparent Energy and Relaxation Frequency. As pointed out above, the cooperation length in dendritic NLO systems is significant, particularly around the poling temperature necessary to achieve acentric ordering. For instance, the entropic energy requirement ($TdS^* \approx E_{a,k} - E_{a,1}$; k = 1, 2) for **TED3** is about 22 and 63 kcal/mol, respectively (Table 3), which is up to twice the enthalpic energy of the arene−pentafluorophenyl interactions involved. In the case of **CE**, the entropic cooperative contribution can be as much 84% of the apparent energy. The apparent (total) energy E_a and the cooperative entropic contribution $T\Delta S^*$ can be evaluated based on the theory of absolute reaction rates applied to relaxations[56,57] via

$$E_a = RT[1 + \ln(k_B T/2\pi h f_p)] + T\Delta S^* = \Delta H^* + T\Delta S^* \tag{3}$$

where k_B represents Boltzmann's constant, h Planck's constant, R the universal gas constant, f_P the peak frequency of the relaxation,[10,38,39,49] and ΔH^* the enthalpic energy component of relaxation. As IFA measurements involve velocities instead of frequencies, a length scale ξ is required between the peak velocity v_p and peak frequency f_p according to the tested relationship[40]

$$\xi = \frac{v_p}{f_p} \tag{4}$$

to benefit fully from eq 3.

Vanishing entropic contributions are found for dendritic NLO materials below T_1, as shown above with Figure 6b for

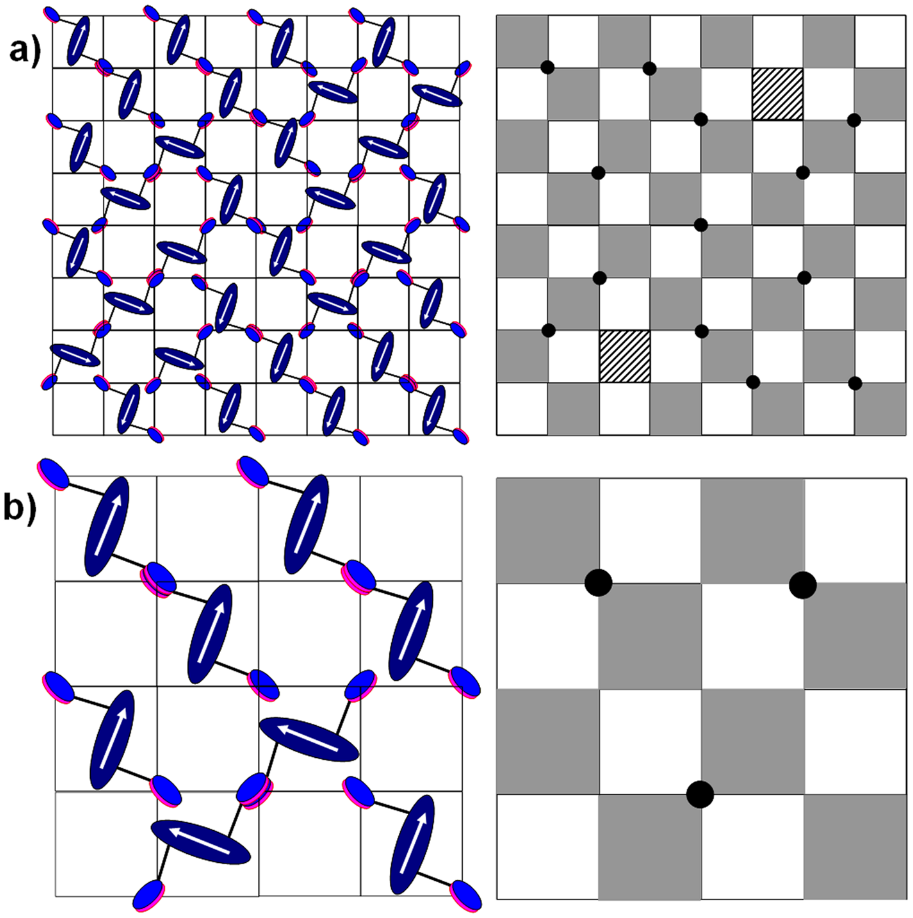

Figure 9. Molecular size effect on the mobility of dendritic NLO molecules. (Left) Densely packed (a) low-molecular-weight system is compared to (b) high-molecular-weight system. The molecules are composed of a core chromophore (arrow indicates dipole moment) and two pendant moieties. (Right) Essence extracted representations of the molecular systems, highlighting the molecules with gray squares, the molecular bonds formed with dark-filled circles, and free molecules with squares with diagonal lines.

CE, and below with Figure 11 for all three material classes, represented by **TED1**, **C1**, and **CE**. Thus, for temperatures below T_1, eq 3 reduces to

$$\Delta H^* = RT[1 + \ln(k_B T/2\pi h f_p)] \tag{5}$$

for dendritic NLO systems. This relationship yields for $E_a \gg RT$ a peak frequency of

$$f_p \approx \frac{kT}{2\pi h} \exp\left(-\frac{E_a}{RT}\right) \tag{6}$$

which works for noncooperative relaxing systems, such as the γ-relaxation (phenyl rotation) in polystyrene.[43,58,59] In dendritic NLO systems, however, this relationship would lead to too low bonding/debonding frequencies that would not result in IFA mode coupling events for the TED molecular systems.

It has recently been estimated that the enthalpic energetic impact of the YLD124 chromophore (Figure 1) is around 20 kcal/mol for **TED1**.[10] Thus, by subtracting the dipolar constraining energies from the apparent energies E_a, pending group bonding/debonding frequencies on the order of 0.1 to 1 ns can be anticipated for the dendritic NLO molecular glasses studied here.

Figure 11 indicates that, above T_1, relaxation processes in all three classes of dendritic materials possess an additional entropic cooperative component, as formally expressed in eq 3, reaching maximum cooperativity at T_2. Above $T_c = T_2 + \Delta T$, with $10 < \Delta T < 20$ °C, (shown here only for **CE**) the cooperative entropic contribution dies out.

Results from Control Systems CC7 and S1. CC7 and **S1** were chosen as control systems, as neither possesses interacting pendant groups. While **CC7** contains a full chromophore that is shielded from neighboring molecules by a "looping alkane chain" to suppress dipole−dipole association, **S1** represents a molecule that partially resembles (at least in size and in aromatic carbon content) the chromophores in this study, but is deprived of a dipole moment. As discussed earlier, both **CC7** and **S1** exhibit only single temperature transitions (dubbed T_2 for consistency), each revealing two thermal regimes of energies, dubbed $E_{a,1}$ and $E_{a,3}$, respectively, for consistency with the previous discussion. The transition results retrieved from Figure 5 and Figure 12a,b, are provided in Table 4.

As expected, the lowest activation energies are found for **S1**. Lacking any obvious means for self-assembly, its transition value T_2 has to be considered a melting transition. In its solid state, below T_2, the low energy value $E_{a,1}$ of 2 ± 1 kcal/mol in **S1** originates from weak van der Waals interaction, i.e., dipolar fluctuations that could be identified either as thermally active modes within the material, or association−dissociation processes between the sample and the probing SFM tip. A mode relaxation frequency on the order of one tenth of a picosecond can be inferred from eq 6 for $E_{a,1}$. Above the melting temperature T_2, a significant increase in energy is

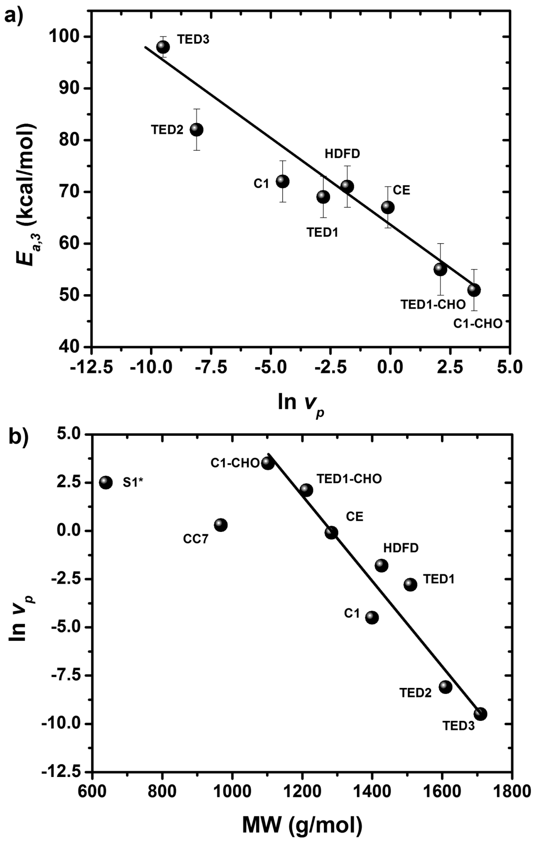

Figure 10. Peak relaxation velocity ln v_p relationships at the reference temperature of 49.5 °C with (a) the apparent activation energy $E_{a,3}$ and (b) the molecular weight MW. Linear fits of molecules with interacting pendant groups reveal for $E_{a,3} = 3.03 \ln v_\mathrm{p} + 63$ and $\ln v_\mathrm{p} -0.022\mathrm{MW} + 27.7$. Contrasted to the linear fit in (b) are molecules with missing pendant groups, i.e., **CC7** and **S1**. For **S1**, * indicates the maximum possible peak value.

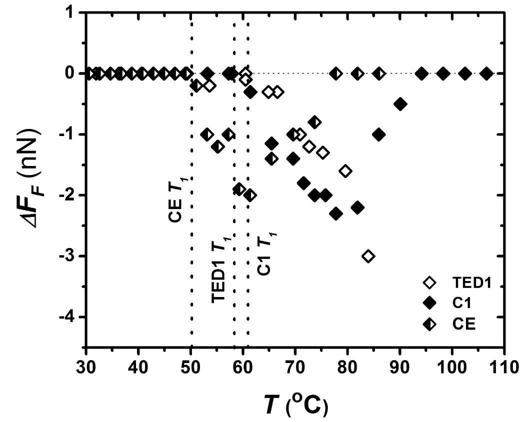

Figure 11. Compilation of the degree of entropic cooperativity $T\Delta S^* \approx -\Delta F_\mathrm{F}/\phi'$ expressed by IFA's vertical friction shifts ΔF_F of representative materials from the three dendritic classes, as defined by Figure 1.

observed, yielding 45 ± 3 kcal/mol. Such high-energy values in the absence of strong interactions can only be explained by entropic contributions, as confirmed by Figure 12b. We will argue that this entropic effect is induced, which is different from the intrinsic cooperativity discussed so far. The lack of a molecular network response in **S1** and an entropic signal ΔF_F that does not vanish at higher temperatures, as found above T_c for the dendritic NLO systems (Figure 11), can only be interpreted as a cantilever probe induced shear alignment effect.

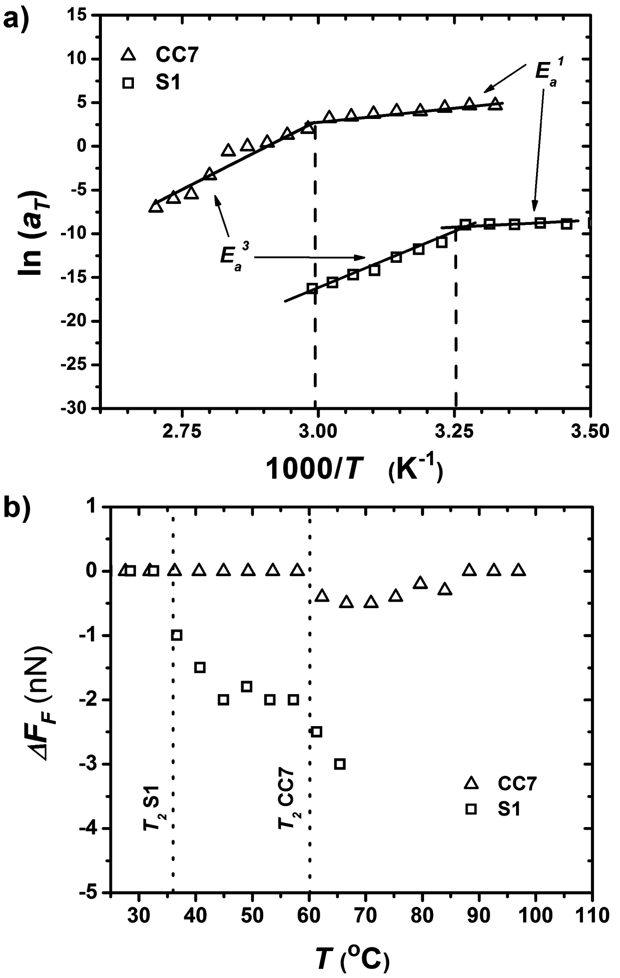

Figure 12. (a) IFA Arrhenius results for **S1** and **CC7**, disclosing the apparent activation energies $E_{a,1}$ and $E_{a,3}$ below and above T_2, respectively, where the reference temperature ($\ln a_\mathrm{T} = 0$) was chosen separately for each data set to space the data for clarity. (b) Vertical ΔF_F shifting plots for **S1** and **CC7**.

Contrary to **S1**, **CC7** is a dipolar chromophore and maintains its solid phase above T_2. The strength of the dipolar interaction of 10 ± 2 kcal/mol determined below T_1 is comparable to the apparent interaction strength observed for **CE** of 11 ± 2 kcal/mol with its hydrogen bond interacting cinnamic ester pendant groups and the chromophore dipole interactions. Comparison between **S1** and **CC7** is the key to understanding the interaction in **CC7**, as **S1** is a nonpolar molecule. The difference in $E_{a,1}$ between these two molecular systems is 8 ± 3 kcal/mol, which provides a measure of the dipole interaction strength for **CC7** below T_1. This finding confirms earlier results[10,23] that were based on comparative findings involving incomplete chromophoric systems, namely, **C1-CHO** and **TED1-CHO**, and their full chromophore counterparts **C1** and **TED1** (Tables 3 and 4). As **CC7** possesses a chromophore with a dipole similar to that of **CE** (calculated as 9.6D and 11.6D, respectively, Tables 3 and 4), we can infer from the energy difference above that about 3 kcal/mol (~25%) of $E_{a,1}$ in **CE** is due to interacting cinnamic ester moiety pendant groups (hydrogen bonding). In comparison, **C1** with its highly interacting mesogenic pendant groups shows an even larger

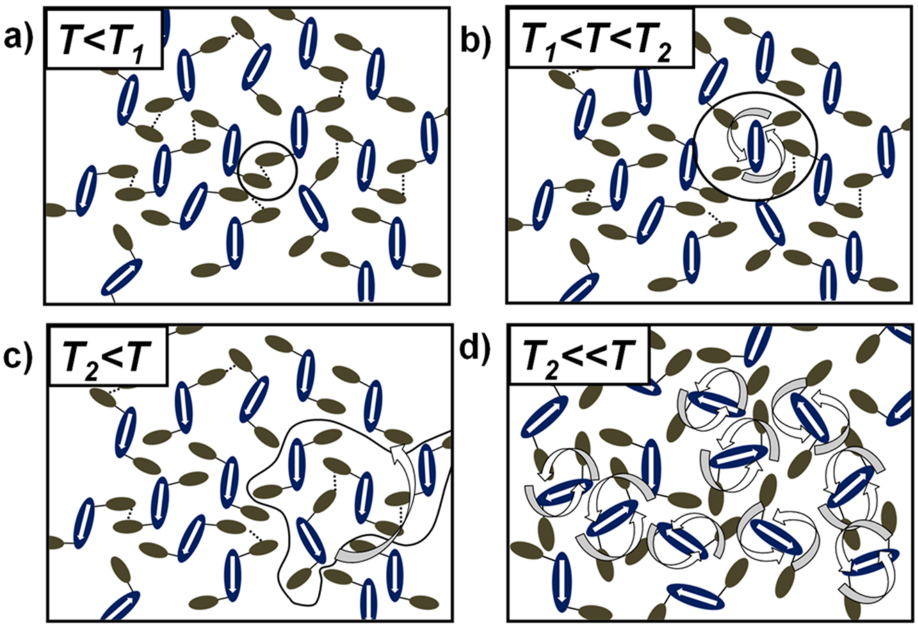

Figure 13. General model of molecular motion in self-assembling dendritic chromophores where dotted lines indicate interacting dendritic groups: (a) $T < T_1$ isolated dendritic side bonding−debonding; (b) $T_1 < T < T_2$, rotational motion allowed by dendritic dissociation; (c) $T_2 < T$ translation of molecules and interacting segments (region within the black line) due to widespread dendritic dissociation; (d) $T_2 \ll T$, uncorrelated translation of molecules where dendritic association is rare.

side group contribution to the glass state below T_1 of about 8 kcal/mol (~50%) based on its $E_{a,1}$ value of 16 ± 2 kcal/mol, as per Table 3.[15,23]

Above T_2, **CC7** reveals an increase followed by a decrease in cooperative entropy (Figure 12b). This qualitative behavior is characteristic for the solid phase of a polymer rubber or melt close to the glass transition. A comparison of the ratio between the **CC7** and **CE** peak values of the ΔF_F shifts and energy values $E_{a,3}$ is of interest. The **CC7**−**CE** comparison yields a ΔF_F peak value ratio of about 1:3, as per Figures 5c and 7b, and an $E_{a,3}$ energy ratio of about 1:1 (based on values taken from Tables 3 and 4). The ratios indicate that the cooperative entropic contribution for NLO materials with interacting pendant side groups is more significant than in merely dipolar interacting systems, suggesting a higher order of mobility. This aspect has been recently confirmed[23] for **C1** with its liquid crystal pendant coumarin side groups, revealing matrix-assisted poling properties, in which the molecular network exhibit a mobility toward higher order.

It can be concluded from the comparison with the two control systems, **S1** and **CC7**, and earlier findings that dendritic groups provide NLO organic glasses with (i) strong phase stabilization, in particular below T_1, (ii) substantial intrinsic entropic cooperativity above T_2, and (iii) structural alignment with mobility toward higher order.

Molecular Phase Description Model. The results and discussion above provide the basis for a molecular model that describes the three phases and two transitions in dendritic NLO molecular glasses (Figure 13). The overall description of the energetics involved, considering also the constraining dipolar fields that emanates from the chromophores (i.e., E_{dipole}), can be expressed as

$$E_a = (RT[1 + \ln(k_B T/2\pi h f_p)] + E_{\text{dipole}}) + T\Delta S^* = \Delta H^* + T\Delta S^* \qquad (7)$$

separating the apparent energy in enthalpic and cooperative entropic components.

Below T_1, the apparent energies $E_{a,1}$ of the three classes of materials reflect the spontaneous bonding−debonding reactions between the dendritic side groups within the dipole field. The process is enthalpic only, as per the IFA vertical shifts (Figure 11). As illustrated in Figure 13a, only isolated associations and dissociations of dendritic bonds (dotted lines) are occurring spontaneously throughout the material phase, leaving the molecular network intact. As the molecules each possess two dendritic groups, molecular mobilities of rotations and translations are statistically non-occurring.

At T_1, a critical number of dendritic association and dissociation events is reached that yield statistically (but only locally available) dissociation of both dendritic bonds of molecules providing them with rotational degrees of freedom (Figure 13b). While the network up to T_2 stays intact, i.e., molecular translation is still subdued, cooperative mobility events are increasingly noticeable with temperature (Figure 11), mainly due to the rotating large dipoles involved. The apparent energy $E_{a,2}$ is now expressed by eq 7, i.e., it contains also a nonzero entropic component of cooperativity.

At T_2, a critical temperature is reached at which the network also accommodates molecular (or molecular chain) translations. This process is highly cooperative near T_2 and gives rise to a high degree of cooperativity expressed through $E_{a,3}$. T_2 has been identified as a glass transition, based on SM-FM and DSC experiments (Figure 4a). With increasing temperature, thermal noise is increasingly disrupting cooperative events, yielding at about 20 °C above T_2 (i.e., T_c) to vanishing cooperativity (Figure 11).

■ SUMMARY AND CONCLUSION

Achieving both high temporal stability and high EO activity is of paramount importance in molecular engineering of novel organic NLO materials. Constraints and high EO active components are built in to achieve this goal, as in this study by dendritic side group interactions, and large heteroaromatic chromophores or polyene bridge chromophores. With cinnamic, coumarin, or arene-perfluoroarene dendritic side groups, it has been shown that the thermal poling regime can be separated neither from the NLO device operating temperature regime ($T < T_1$) nor from the dipole annihilation regime at high temperatures ($T > T_2$) that are known to lead to antiparallel dipole pairing. As described in the model above (Figure 13b), the origin for the existence of such a unique intermediate phase regime can be attributed to the association—dissociation mechanism of the dual bonds, through which the dendritic molecules interact. Within the intermediate temperature regime, $T_1 < T < T_2$, and close to T_2, where molecular (rotational) mobilities are entropically highly cooperative, thermal electric field poling is most effective and beneficial for achieving a lower dimensional organization, such as an acentric chromophore order.

Considering the energetic information (Table 3 and Figure 7), we find the width of the intermediate thermal regime to coincide with an increase in the interaction strength of the pendant groups. In other words, while the interaction strength is beneficial to the stability of the poled molecular system under NLO operation by raising T_1,[10] it negatively impacts the thermal window of opportunity to acentrically align the chromophores during thermally activated poling. These two competing conclusions summarize the findings above and are captured in the plot of Figure 14 that relates the poling efficiency (defined as the poling field, E_p, normalized EO activity coefficient, r_{33}) to the enthalpic activation energy $E_{a,1}$. The latter is generally indicative of stability,[10] and affects the width of the intermediate temperature regime. Materials with excellent stability and initial EO activity will be high on both axes, i.e., in the top-right region of the plot. As discussed above based on Tables 1 and 2, the width of the intermediate thermal transition regime depends on (a) the size of the chromophore, i.e., increasing for smaller chromophores, as shown with **TED1-CHO** and **C1-CHO**, and (b) pendant group interaction strength, decreasing with increasing strength, as found for with **CE** and **C1**, and **TED1**, **TED2** to **TED3**.

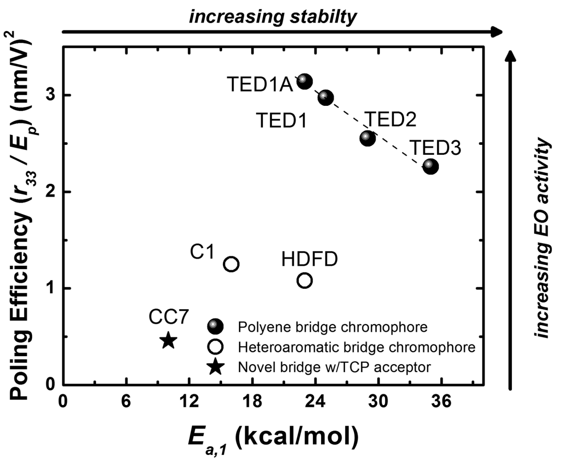

Figure 14. Poling efficiencies[9,14,23] as a function of $E_{a,1}$ for various materials poled on ITO-coated glass, revealing the competition of EO activity and stability.

As shown in Figure.14, the poling efficiency is also greatly impacted by the type of chromophores incorporated into the molecules. Polyene bridge-type chromophores employed in the TED series have been shown to produce higher r_{33} values than their heteroaromatic counterparts,[9] accounting for the higher poling efficiency values for the TED series.

Thus, it has been shown that the presence of dendritic groups fundamentally alters the observed transition temperatures and molecular relaxation behavior. Interacting dendritic groups introduce an intermediate phase regime bordered by two thermal transitions. The temperature gap between the two transitions was found to be substantially widened by the presence of chromophores. Molecules lacking dendrons showed only one transition whether or not chromophores were present. Low-temperature relaxation activation energies, which correspond to long-term stability, followed the trend: cinnamic ester groups, coumarin moieties, followed by arene-perfluoroarene interacting groups, indicating the relative strength of these interactions within the molecular glass. Intermolecular interactions definitely improved the phase long term stability and are expected to do so in the poled state as well. Interestingly, dendritic glasses show a universal trend in peak relaxation velocity as a function of both molecular weight and activation energy, indicating that molecular size heavily influences behavior due to the density of interacting dendritic groups. It was also argued that dendritic groups provide NLO organic glasses with structural alignment with mobility toward higher order.

This study showed the importance of entropic cooperativity in the design of novel materials that entail a multitude of interactive constraints form dipole field interactions to local dendritic bonding. To further our understanding on how to effectively translate this information in future molecular designs of self-assembling organic systems is part of our ongoing studies.

■ AUTHOR INFORMATION

Corresponding Author

*E-mail: roverney@u.washington.edu.

Notes

The authors declare no competing financial interest.

■ ACKNOWLEDGMENTS

This work was supported by a University Initiative Fund (UIF) graduate fellowship through the Center for Nanotechnology (CNT) at the University of Washington. D. B. Knorr thanks ARCS for a graduate fellowship. Funding support from the National Science Foundation (DMR-0905686) and the Air Force Office of Scientific Research (FA9550-09-1-0589 MOD) is gratefully acknowledged. C. Zhang is obliged to the support from National Science Foundation (EEC 0812072) and the NNIN Laboratory Experience for Faculty (LEF) Program at the University of Washington.

■ REFERENCES

(1) Kajzar, F.; Lee, K.-S.; Jen, A. K.-Y. *Adv. Polym. Sci.* **2003**, *161* (Polymers for Photonics Applications II), 1−85.

(2) Ma, H.; Jen, A. K.-Y.; Dalton, L. R. *Adv. Mater.* **2002**, *14*, 1339−1365.

(3) Dalton, L. R.; Steier, W. H.; Robinson, B. H.; Zhang, C.; Ren, A.; Garner, S.; Chem, A.; Londergan, T.; Irwin, L.; Carlson, B.; et al. *J. Mater. Chem.* **1999**, *9*, 1905−1920.

(4) Marder, S. R.; Kippelen, B.; Jen, A. K. Y.; Peyghambarian, N. *Nature* **1997**, *388*, 845−851.

(5) Shi, Y.; Zhang, C.; Zhang, H.; Bechtel, J. H.; Dalton, L. R.; Robinson, B. H.; Steier, W. H. *Science* **2000**, *288*, 119−122.
(6) Robinson, B. H.; Dalton, L. R. *J. Phys. Chem. A* **2000**, *104*, 4785−4795.
(7) Benight, S. J.; Robinson, B. H.; Dalton, L. R. Nano-engineering of Molecular Interactions in Organic electro-Optic Materials. In *Molecular Interactions*, Meghea, A., Ed.; InTech: Rijeka, Croatia, 2012.
(8) Dalton, L. R.; Benight, S. J.; Johnson, L. E.; Knorr, D. B.; Kosilkin, I.; Eichinger, B. E.; Robinson, B. H.; Jen, A. K. Y.; Overney, R. M. *Chem. Mater.* **2011**, *23*, 430−445.
(9) Zhou, X.-H.; Luo, J.; Huang, S.; Kim, T.-D.; Shi, Z.; Cheng, Y.-J.; Jang, S.-H.; Knorr, D. B., Jr.; Overney, R. M.; Jen, A. K. Y. *Adv. Mater.* **2009**, *21*, 1976−1981.
(10) Knorr, D. B.; Zhou, X. H.; Shi, Z. W.; Luo, J. D.; Jang, S. H.; Jen, A. K. Y.; Overney, R. M. *J. Phys. Chem. B* **2009**, *113*, 14180−14188.
(11) Gray, T.; Kim, T.-D.; Knorr, D. B., Jr.; Luo, J.; Jen, A. K. Y.; Overney, R. M. *Nano Lett.* **2008**, *8*, 754−759.
(12) Gray, T.; Killgore, J. P.; Luo, J.; Jen, A. K.-Y.; Overney, R. M. *Nanotechnology* **2007**, *18*, 044009.
(13) Luo, J.; Liu, S.; Haller, M.; Liu, L.; Ma, H.; Jen, A. K.-Y. *Adv. Mater.* **2002**, *14*, 1763−1768.
(14) Kim, T.-D.; Kang, J.-W.; Luo, J.; Jang, S.-H.; Ka, J.-W.; Tucker, N.; Benedict, J. B.; Dalton, L. R.; Gray, T.; Overney, R. M.; et al. *J. Am. Chem. Soc.* **2007**, *129*, 488−489.
(15) Benight, S. J.; Johnson, L. E.; Barnes, R.; Olbricht, B. C.; Bale, D. H.; Reid, P. J.; Eichinger, B. E.; Dalton, L. R.; Sullivan, P. A.; Robinson, B. H. *J. Phys. Chem. B* **2010**, *114*, 11949−11956.
(16) Benight, S. J.; Bale, D. H.; Olbricht, B. C.; Dalton, L. R. *J. Mater. Chem.* **2009**, *19*, 7466−7475.
(17) Hah, H.; Sung, S.-J.; Cho, K. Y.; Park, J.-K. *Polym. Bull.* **2008**, *61*, 383−390.
(18) Li, W. J.; Lynch, V.; Thompson, H.; Fox, M. A. *J. Am. Chem. Soc.* **1997**, *119*, 7211−7217.
(19) Yu, Y.-J.; Lee, S.-H.; Choi, D. H.; Jin, J.-I.; Tessler, N. *Macromol. Res.* **2007**, *15*, 142−146.
(20) Tian, Y. Q.; Akiyama, E.; Nagase, Y.; Kanazawa, A.; Tsutsumi, O.; Ikeda, T. *J. Mater. Chem.* **2004**, *14*, 3524−3531.
(21) Tian, Y. Q.; Kong, X. X.; Nagase, Y.; Iyoda, T. *J. Polym. Sci., Part A: Polym. Chem.* **2003**, *41*, 2197−2206.
(22) Dalton, L.; Benight, S. *Polymers* **2011**, *3*, 1325−1351.
(23) Benight, S. J.; Knorr, D. B.; Johnson, L. E.; Sullivan, P. A.; Lao, D.; Sun, J.; Kocherlakota, L. S.; Elangovan, A.; Robinson, B. H.; Overney, R. M.; Dalton, L. R. *Adv. Mater.* **2012**, *24*, 3263−3268.
(24) Shen, K. H.; Kim, J. H.; Kim, G. W.; Cho, M. J.; Lee, S. K.; Choi, D. H. *Macromol. Res.* **2005**, *13*, 180−186.
(25) Legge, C. H.; Whitcombe, M. J.; Gilbert, A.; Mitchell, G. R. *J. Mater. Chem.* **1991**, *1*, 303−304.
(26) Palinko, I. *Acta Crystallogr., Sect. B: Struct. Sci.* **1999**, *55*, 216−220.
(27) Kortvelyesi, T.; Palinko, I. *Theochem* **2000**, *531*, 99−103.
(28) Pires, D.; Hedrick, J. L.; De Silva, A.; Frommer, J.; Gotsmann, B.; Wolf, H.; Despont, M.; Duerig, U.; Knoll, A. W. *Science* **2010**, *328*, 732−735.
(29) Luo, J.; Huang, S.; Cheng, Y.-J.; Kim, T.-D.; Shi, Z.; Zhou, X.-H.; Jen, A. K.-Y. *Org. Lett.* **2007**, *9*, 4471−4474.
(30) Bhatt, S.; Nayak, S. K. *Synth. Commun.* **2007**, *37*, 1381−1388.
(31) He, M.; Leslie, T. M.; Sinicropi, J. A. *Chem. Mater.* **2002**, *14*, 4662−4668.
(32) Pond, S. J. K.; Rumi, M.; Levin, M. D.; Parker, T. C.; Beljonne, D.; Day, M. W.; Bredas, J. L.; Marder, S. R.; Perry, J. W. *J. Phys. Chem. A* **2002**, *106*, 11470−11480.
(33) Sills, S. E.; Overney, R. M.; Chau, W.; Lee, V. Y.; Miller, R. D.; Frommer, J. *J. Chem. Phys.* **2004**, *120*, 5334.
(34) Overney, R. M.; Buenviaje, C.; Luginbuhl, R.; Dinelli, F. *J. Therm. Anal. Cal.* **2000**, *59*, 205−225.
(35) Buenviaje, C. K.; Ge, S. R.; Rafailovich, M. H.; Overney, R. M. *Mater. Res. Soc. Symp. Proc.* **1998**, *552*, 187−192.
(36) Wei, J. H.; He, M. Y.; Overney, R. M. *J. Membr. Sci.* **2006**, *279*, 608−614.
(37) Gu, X.; Knorr, D. B., Jr.; Wang, G.; Overney, R. M. *Thin Solid Films* **2011**, *519*, 5955−5961.
(38) Knorr, D. B. J.; Gray, T.; Overney, R. M. *Ultramicroscopy* **2009**, *109*, 991−1000.
(39) Knorr, D. B., Jr.; Widjaja, P.; Acton, O.; Overney, R. M. *J. Chem. Phys.* **2011**, *134*, 104502.
(40) Sills, S.; Gray., T.; Overney, R. M. *J. Chem. Phys.* **2005**, *123*, 134902.
(41) Ferry, J. D. Dependence of viscoelastic behavior on temperature and pressure. In *Viscoelastic Properties of Polymers*; John Wiley & Sons: New York, 1980; Chapter 11.
(42) Ward, I. M. *Mechanical Properties of Solid Polymers*; Wiley-Interscience: London, 1971.
(43) Sills, S.; Overney, R. M. *Phys. Rev. Lett.* **2003**, *91*, 095501.
(44) Pople, J. A.; Santry, D. P. *J. Chem. Phys.* **1965**, *43*, S129.
(45) Dewar, M. J. S.; Yuan, Y. C. *Inorganic Chemistry* **1990**, *29*, 3881−3890.
(46) Dewar, M. J. S.; Zoebisch, E. G. *THEOCHEM* **1988**, *180*, 1−21.
(47) Dewar, M. J. S.; Zoebisch, E. G.; Healy, E. F.; Stewart, J. J. P. *J. Am. Chem. Soc.* **1985**, *107*, 3902−3909.
(48) Kiss, J. T.; Felföldi, K.; Körtvélyesi, T.; Pálinkó, I. *Vibr. Spectrosc.* **2000**, *22*, 63−73.
(49) Knorr, D. B. J.; Gray, T.; Overney, R. M. *J. Chem. Phys.* **2008**, *129*, 074504.
(50) Patrick, C. R.; Prosser, G. S. *Nature* **1960**, *187*, 1021−1021.
(51) Smith, V. B.; Massey, A. G. *Tetrahedron* **1969**, *25*, 5495−5501.
(52) Weck, M.; Dunn, A. R.; Matsumoto, K.; Coates, G. W.; Lobkovsky, E. B.; Grubbs, R. H. *Angew. Chem., Int. Ed.* **1999**, *38*, 2741−2745.
(53) Collings, J. C.; Roscoe, K. P.; Robins, E. G.; Batsanov, A. S.; Stimson, L. M.; Howard, J. A. K.; Clark, S. J.; Marder, T. B. *New J. Chem.* **2002**, *26*, 1740−1746.
(54) Kishikawa, K.; Oda, K.; Aikyo, S.; Kohmoto, S. *Angew. Chem., Int. Ed.* **2007**, *46*, 764−768.
(55) Watt, S. W.; Dai, C.; Scott, A. J.; Burke, J. M.; Thomas, R. L.; Collings, J. C.; Viney, C.; Clegg, W.; Marder, T. B. *Angew. Chem., Int. Ed.* **2004**, *43*, 3061−3063.
(56) Starkweather, H. W., Jr. *Macromolecules* **1981**, *14*, 1277−1281.
(57) Starkweather, H. W., Jr. *Macromolecules* **1988**, *21*, 1798−1802.
(58) Arrese-Igor, S.; Arbe, A.; Frick, B.; Colmenero, J. *Macromolecules* **2011**, *44*, 3161−3168.
(59) Yano, O.; Wada, Y. *J. Polym. Sci., Part A: Polym. Phys.* **1971**, *9*, 669−686.